Contractile Smooth Muscle and Active Stress Generation in Porcine Common Carotids

Boran Zhou
Department of Radiology,
Mayo Clinic College of Medicine,
Rochester, MN 55905

David A. Prim
College of Engineering and Computing, Biomedical Engineering Program,
University of South Carolina,
Columbia, SC 29208

Eva J. Romito
College of Engineering and Computing, Biomedical Engineering Program,
University of South Carolina,
Columbia, SC 29208;
Cardiovascular Translational Research Center,
University of South Carolina,
Columbia, SC 29208

Liam P. McNamara
College of Engineering and Computing, Biomedical Engineering Program,
University of South Carolina,
Columbia, SC 29208

Francis G. Spinale
Cardiovascular Translational Research Center,
University of South Carolina,
Columbia, SC 29208;
School of Medicine, Department of Cell Biology and Anatomy,
University of South Carolina,
Columbia, SC 29208

Tarek Shazly
College of Engineering and Computing, Biomedical Engineering Program,
University of South Carolina,
Columbia, SC 29208;
College of Engineering and Computing,
Department of Mechanical Engineering,
University of South Carolina,
Columbia, SC 29208

John F. Eberth[1]
College of Engineering and Computing,
Biomedical Engineering Program,
University of South Carolina,
Columbia, SC 29208;
School of Medicine, Department of Cell Biology and Anatomy,
University of South Carolina,
Columbia, SC 29208
e-mail: john.eberth@uscmed.sc.edu

The mechanical response of intact blood vessels to applied loads can be delineated into passive and active components using an isometric decomposition approach. Whereas the passive response is due predominantly to the extracellular matrix (ECM) proteins and amorphous ground substance, the active response depends on the presence of smooth muscle cells (SMCs) and the contractile machinery activated within those cells. To better understand determinants of active stress generation within the vascular wall, we subjected porcine common carotid arteries (CCAs) to biaxial inflation–extension testing under maximally contracted or passive SMC conditions and semiquantitatively measured two known markers of the contractile SMC phenotype: smoothelin and smooth muscle-myosin heavy chain (SM-MHC). Using isometric decomposition and established constitutive models, an intuitive but novel correlation between the magnitude of active stress generation and the relative abundance of smoothelin and SM-MHC emerged. Our results reiterate the importance of stretch-dependent active stress generation to the total mechanical response. Overall these findings can be used to decouple the mechanical contribution of SMCs from the ECM and is therefore a powerful tool in the analysis of disease states and potential therapies where both constituent are altered.
[DOI: 10.1115/1.4037949]

Keywords: arterial mechanics, biaxial active response, active stress, smooth muscle cells (SMC), common carotid artery (CCA)

Introduction

The passive mechanical response of blood vessels undergoing inflation–extension testing demonstrates a nonlinear stress–stretch relationship due to the heterogeneous nature and inherent undulation of existing extracellular matrix (ECM) proteins. Whereas passive mechanics have been effectively modeled within the framework of nonlinear finite elasticity via biaxial mechanical testing, quantitative histology, and the subsequent identification of constitutive mechanical properties; studies of the active mechanical response have been fundamentally different. The most common approach has been empirical identification of active stress–strain relations when smooth muscle cells (SMCs) are stimulated to contract [1,2].

Acute chemomechanical stimuli are capable of triggering vascular SMCs to initiate their contractile state in vivo, resulting in a change in vessel geometry (lumen constriction or dilation). Although the majority of SMCs in the healthy vascular wall are of the contractile phenotype, SMCs are capable of modulating toward a synthetic or proliferative status such as that which is commonly observed in carotid artery disease. This phenotypic modulation dramatically affects the capacity of SMCs to generate active stresses and modify vascular tone [3]. There are surprisingly few biaxial studies focused on the correlation between SMC markers and the resultant isometric active stress generation [4,5]. The aims of this study are two-fold. First, an integrated experimental-theoretical approach was utilized to assess the passive and active biaxial mechanical responses of common carotid arteries (CCAs). Inherent to the completion of this aim is the identification of parameters used in the established constitutive formulations [6–9]. Second, semiquantitative histology was performed to enable correlation between the contractile SMC content and active circumferential stress generation of CCAs that were stimulated to maximally contract. Building on the pioneering efforts of earlier investigations that have used biochemical stimulants to induce vascular tone, here we present a comprehensive mechanical analysis that relates active mechanics to markers of contractile SMC phenotype [10,11].

Materials and Methods

Vessel Isolation and Biomechanical Testing. All animal procedures were approved by the Institute Animal Care and Use

[1]Corresponding author.
Manuscript received May 17, 2017; final manuscript received September 14, 2017; published online November 9, 2017. Assoc. Editor: Guy M. Genin.

Committee at the University of South Carolina. Adult male Yorkshire pigs weighing approximately 25 kg (8 weeks old, $n = 6$) were anesthetized with sodium pentobarbital and the CCAs were isolated and dissected from perivascular tissue. Prior to, and immediately following excision, the distances between the proximal and distal ends of the vessel were measured and recorded using a digital caliper. Arteries were then gently rinsed and cannulated within the Bose BioDynamic 5270 mechanical testing device using a sterile 4–0 suture. The samples were submerged and continuously perfused with aerated (95% $O_2 + 5\%CO_2$) Krebs–Henseleit solution at 37 °C and *p*H of 7.4. The maximally contracted state was induced by adding 10^{-5} M epinephrine to the circulating medium followed by a 15 min acclimation period [4]. Then, samples underwent five cycles of preconditioning consisting of pressurization from 20 to 200 mmHg (1.5 mmHg/s) at the in situ axial stretch ratio. Blood vessels were then quasi-statically pressurized (0–200 mmHg, 20 mmHg steps, 10 s/step) over three cycles and at three levels of axial stretch spanning the in situ axial stretch ratio, with the outer diameter and axial force recorded at each experimental state via integrated system components and software (Wintest 4.1, Bose ElectroForce, Eden Prairie, MN and LabVIEW 2010, National Instruments Corporation, Austin, TX). To assess the mechanical response under fully relaxed SMCs, the circulating medium was flushed and replaced with Krebs–Henseleit solution containing 10^{-5} M sodium nitroprusside (SNP). This molar concentration of SNP has been shown to completely ameliorate vascular smooth muscle tone [10]. Following another 15 min acclimation period, identical mechanical preconditioning and biaxial mechanical testing protocols were repeated. Then, ring slices were prepared (1 mm width) and a stress relieving cut introduced so that the thickness (H), opening angle (OA) and the inner and outer arc lengths (L_i, L_o) could be measured or calculated (Table 1). The inner radii (r_i) at any deformed state could then be calculated from the incompressibility assumption provided the outer radii (r_o) is known. The midwall circumferential and axial stretch ratios are defined as

$$\lambda_\theta = \frac{2\pi(r_o - r_i)}{L_o + L_i}, \quad \lambda_z = \frac{\ell}{L} \tag{1}$$

where ℓ and L are the loaded and unloaded lengths of the vessel segment, respectively. The kinematics associated with this deformation can be found in other publications [4,12].

Theoretical Framework. Common carotid arteries are modeled as cylindrically orthotropic, elastic, incompressible solids, under a state of axisymmetric deformation with the wall stress divisible into active and passive components. Following a hybrid two-dimensional/three-dimensional approach, the constitutive relationships for the total stresses are defined by Ref. [4]

$$\sigma_\theta^t = \sigma_r + \lambda_\theta \frac{\partial W}{\partial \lambda_\theta} + \sigma_\theta^a, \quad \sigma_z^t = \sigma_r + \lambda_z \frac{\partial W}{\partial \lambda_z} + \sigma_z^a \tag{2}$$

where the radial stress σ_r must be determined from the equilibrium and boundary conditions. Subscripts θ, r, and z indicate circumferential, radial, and axial directions, while t and a indicate the total and active stresses, respectively. $W = W(\lambda_\theta, \lambda_z)$ is the strain energy function that characterizes the passive mechanical properties of the arterial wall.

Table 1 Geometrical parameters of the zero stress configuration for each arterial sample in the fully relaxed SMC state

Sample	R_i (mm)	H (mm)	OA (deg)	L_o (mm)	L_i (mm)	λ_z^{iv}
1	3.33	0.88	100	11.7	9.27	1.70
2	4.18	1.31	86.2	18.1	13.8	1.70
3	3.28	0.92	93.0	12.7	9.94	1.70
4	2.26	0.79	77.3	10.9	8.09	1.42
5	1.31	0.98	17.8	12.9	7.39	1.45
6	3.53	0.90	96.9	12.7	10.1	1.45
Average	2.98	0.96	78.6	13.2	9.77	1.57
SD	0.94	0.16	28.2	2.32	2.05	0.13

We assume that the stress distributions across the wall are nearly uniform, and therefore mean stress and strain values adequately represent experimental states. Accordingly, hereafter stresses refer to mean values calculated from experimental data using

$$\sigma_r = -P\frac{r_i}{r_i + r_o}, \quad \sigma_\theta = P\frac{r_i}{r_o - r_i}, \quad \sigma_z = \frac{f}{\pi\left(r_o^2 - r_i^2\right)} \tag{3}$$

where r_o is the deformed outer radius and f is the axial force.

Active stresses are then computed via isometric comparisons between fully relaxed and maximally contracted SMC states. The active circumferential and axial stresses are, therefore, calculated as

$$\sigma_\theta^a = \sigma_\theta^{ic} - \sigma_\theta^p + \sigma_r^p - \sigma_r^{ic}, \quad \sigma_z^a = \sigma_z^{ic} - \sigma_z^p + \sigma_r^p - \sigma_r^{ic} \tag{4}$$

where the superscript ic signifies the isometric contracted state and p the passive state. Therefore, combining Eqs. (3) and (4), the active stresses are directly calculated using

$$\sigma_\theta^a = \frac{2r_i r_o}{r_o^2 - r_i^2}(P_{ic} - P_p) \quad \sigma_z^a = \frac{f_{ic} - f_p}{\pi\left(r_o^2 - r_i^2\right)} + \frac{r_i}{r_i + r_o}(P_{ic} - P_p) \tag{5}$$

where P_p and P_{ic} are the pressures and f_p and f_{ic} the forces in the passive and isometric contraction states, respectively.

The passive mechanical properties of CCAs were modeled via a structure-motivated strain energy function W of the form [13]

$$W = c(I_1 - 3) + \sum_{k=1,2,3,4} \frac{b_{1k}}{2b_{2k}}\left\{\exp\left[b_{2k}\left(\lambda_k^2 - 1\right)^2\right] - 1\right\} \tag{6}$$

and has previously been shown to be a good descriptor of passive mechanics without being over-parameterized [14]. The first term in W accounts for the isotropic contribution of elastin [15] with a material constant, c and the first invariant of the Cauchy–Green strain tensor, $I_1 = \lambda_\theta^2 + \lambda_z^2 + (\lambda_\theta\lambda_z)^{-2}$. The second term includes the contribution of k (four) families of collagen fibers with a specific orientation angle α_k (such that $k = 1,2,3,4$), defined with respect to the longitudinal axis where $\alpha_{k=1}$ and $\alpha_{k=2}$ represent the circumferentially ($\alpha_{k=1} = 90$ deg) and axially ($\alpha_{k=2} = 0$ deg) oriented fiber families. We further assume that the diagonal fibers for the remaining two families have equal but opposite angles, where $\alpha_{k=3} = -\alpha_{k=4}$, b_{1k}, and b_{2k} are material constants, and thus $b_{13} = b_{14}$ and $b_{23} = b_{24}$. The stretch ratio experienced by each family of collagen fibers due to deformation is $\lambda_k = \sqrt{\lambda_\theta^2 \sin^2\alpha_k + \lambda_z^2 \cos^2\alpha_k}$. Unknown material constants are determined by minimization of the objective function

$$\Omega_p = \sum_{n=1}^{N}\left(\frac{\hat{\sigma}_{\theta n}^T - \hat{\sigma}_{\theta n}^E}{\hat{\sigma}_{\theta n}^E}\right)^2 + \sum_{n=1}^{N}\left(\frac{\hat{\sigma}_{zn}^T - \hat{\sigma}_{zn}^E}{\hat{\sigma}_{zn}^E}\right)^2 \tag{7}$$

where $n = 1, 2, \ldots, N$ is the number of the experimental states and

$$\hat{\sigma}_\theta^E = P_p\frac{r_i}{r_o - r_i} + P_p\frac{r_i}{r_o + r_i}, \quad \hat{\sigma}_z^E = \frac{f_p}{\pi\left(r_o^2 - r_i^2\right)} + P_p\frac{r_i}{r_o + r_i} \tag{8}$$

and

Table 2 Best-fit parameters for the utilized structure-motivated strain energy function for the passive mechanical response

Sample	C (Pa)	b_{11} (Pa)	b_{21}	b_{12} (Pa)	b_{22}	$b_{13} = b_{14}$ (Pa)	$b_{23} = b_{24}$	$\alpha_3 = -\alpha_4$ (deg)	R^2
1	111	2280	0.20	1480	0.20	100	1.10	30.2	0.90
2	13,800	11,000	0.20	100	0.60	100	0.70	27.4	0.90
3	7680	215	0.40	1240	0.50	98.9	0.90	44.8	0.40
4	7170	507	1.30	5680	1.10	101	3.40	35.8	0.40
5	108	1690	0.50	1600	0.80	102	2.10	30.4	1.30
6	106	1030	0.58	630	1.45	101	2.16	35.6	0.73
Average	4830	2770	0.53	1790	0.76	101	1.74	34.0	0.78
SD	5180	3730	0.35	1810	0.40	0.88	0.91	5.67	0.32

Table 3 Best-fit parameters for the proposed model of the circumferential active stresses

						Range over which model is valid	
Sample	S_θ (kPa)	β_θ	$\lambda_{\theta,\max}$	$\lambda_{\theta,0}$	R^2	λ_θ	λ_z
1	151	0.66	1.87	1.08	0.98	(1.08, 1.87)	(1.6, 1.8)
2	54.8	0.83	1.59	0.89	0.77	(0.89, 1.59)	(1.6, 1.8)
3	73.4	0.76	1.95	1.09	0.83	(1.09, 1.95)	(1.6, 1.8)
4	94.8	1.90	2.58	0.83	0.61	(0.83, 2.58)	(1.4, 1.5)
5	31.7	2.01	1.79	1.19	0.75	(1.19, 1.79)	(1.4, 1.5)
6	24.8	2.00	1.98	1.33	0.68	(1.33, 1.98)	(1.4, 1.5)
Average	71.7	1.36	1.96	1.07	0.77		
SD	42.5	0.61	0.31	0.17	0.12		

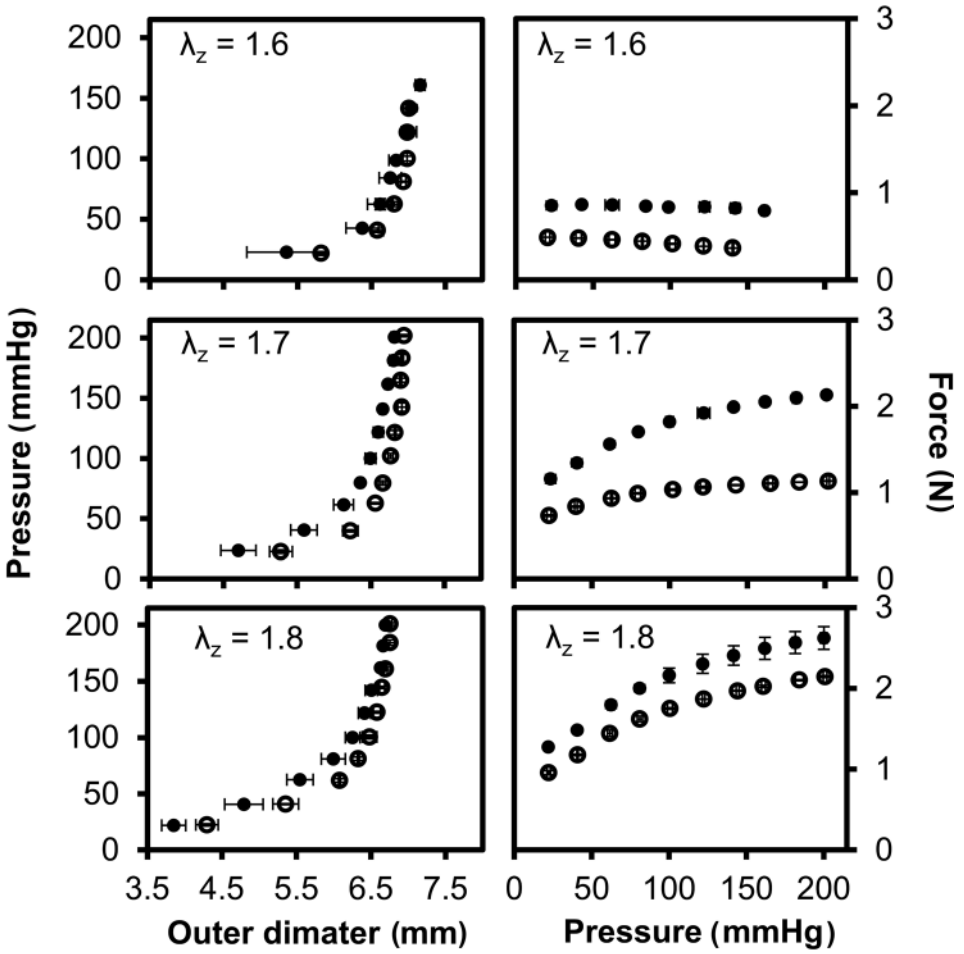

Fig. 1 Pressure-deformed outer diameter (left) and axial force-pressure (right) relationships for a representative porcine common carotid artery (sample 3). The mechanical response was recorded under conditions of maximally contracted (•) and fully relaxed (○) SMC states, and at three axial stretch ratios (λ_z) that span the in situ value. Error bars represent the standard deviation of three repeat measurements on the same vessel.

$$\hat{\sigma}_\theta^T = \lambda_\theta \frac{\partial W}{\partial \lambda_\theta}, \quad \hat{\sigma}_z^T = \lambda_z \frac{\partial W}{\partial \lambda_z} \tag{9}$$

Superscripts T and E refer to theoretical and experimental values, respectively.

Analytical Form for the Active Stress–Stretch Relationship. We assume that the active stress in the circumferential direction depends on stretch ratios, i.e., $\sigma_\theta^a = \sigma_\theta^a(\lambda_\theta, \lambda_z)$, and apply the following constitutive relation [9]:

$$\sigma_\theta^a = S_\theta(\beta_\theta \lambda_z - 1)\lambda_\theta \left[1 - \left(\frac{\lambda_{\theta\max} - \lambda_\theta}{\lambda_{\theta\max} - \lambda_{\theta o}}\right)^2\right] \tag{10}$$

where S_θ is an activation parameter with units of stress; $\lambda_{\theta\max}$ is the stretch at which the maximal active circumferential stresses are developed; $\lambda_{\theta o}$ is the stretch below which no active stresses are generated; and β_θ is a material constant that relates the active stresses in the circumferential direction to axial stretches. Model parameterization was achieved via minimization of the objective function

$$\Omega_\theta = \sum_{n=1}^{N} \left(\frac{\sigma_\theta^{a(\text{theo})} - \sigma_\theta^{a(\text{exp})}}{\sigma_\theta^{a(\text{exp})}}\right)_n^2 \tag{11}$$

The resulting material constants and residuals for both minimization problems are reported in Tables 2 and 3.

Histological Quantification. Specimens were fixed in the unloaded state in 4% paraformaldehyde, embedded in paraffin blocks, and cut to approximately 5 μm sections using a microtome. Alternating sections were stained for Verhoeff's elastic fiber counterstained with methyl blue, Hematoxylin and Eosin (H&E), smoothelin, or smooth muscle-myosin heavy chain (SM-MHC). Mouse monoclonal antismoothelin antibody (R4A) and rabbit polyclonal anti-SM-MHC 11 antibody were obtained from Abcam (Cambridge, MA). Antibodies were stained using a Dako (Carpinteria, CA) immune-peroxidase kit with 3,3′-diaminobenzidinetrahydrochloride (DAB) as the peroxidase substrate. All samples were stained together to prevent batch-to-batch variations and imaged under consistent lighting conditions. A Nikon E600 microscope with CCD camera and computer interface with Q Capture (QImaging) recorded all images. Each slide ($n = 4$ for each vessel) was imaged in at least three locations. Image thresholding was conducted to compare pixels stained positive for contractile SMCs—as represented by immuno-stained brown smoothelin or SM-MHC—to total tissue pixels from the H&E image using ImageJ software (National Institutes of Health, Bethesda, MD) with the "Threshold_Colour" plugin ($H = 80$–215 deg, $S = 0.25$–1.0, and $V = 0.0$–1.0). Each total tissue area was saved as a region of interest, which was then superimposed on the corresponding immunohistochemistry slides to estimate pixel area density (area positively stained pixels/area all tissue pixels) [16,17]. Protein analysis was performed in this manner, rather than using a Western Blot, to identify spatial differences in organization of contractile markers and is supported by a number of prior studies [18–20].

Results and Discussion

The aims of this study were to quantify the active and passive mechanical response of porcine CCAs to biaxial loading (Figs. 1 and 2), to implement established constitutive equations for the active and passive mechanical properties of these arteries (Tables 2 and 3), and to evaluate the relationship between active stress generation and two histological markers of SMC phenotype: smoothelin and SM-MHC (Figs. 3 and 4). Mechanical testing followed previously defined protocols [1,2,6,11] and theoretical modeling implemented contemporary approaches to deciphering active mechanics [4,5,9]. A tremendous advantage enabled by this approach is the capacity to isolate the passive (ECM based) from the active (contractile SMC based) contributions to the total stress state. This delineation has an important role in deciphering disease states that affect both the contractile capacity of SMCs and the stiffness of the ECM.

Smooth muscle cell phenotype exists as a spectrum in both the healthy and diseased vascular wall [3,21]. Two established markers used to indicate contractile phenotype are smoothelin and SM-MHC [22], while specific markers of synthetic/proliferative SMCs are often more difficult to ascertain [23]. Smoothelin is expressed only by contractile SMCs and plays a role in regulating and stabilizing contractile structures [21,24], while SM-MHC is directly involved in the process of contraction [3,22]. Other contractile markers such as alpha smooth muscle actin are less specific and may be found in other cell types. Although apparent in the reported specimen (Figs. 3(*c*) and 3(*d*)), DAB staining intensity was not quantified as a separate variable. Instead pixels were simply considered as positively or negatively stained based on ranges determined by the thresholding analysis (see insets of Figs.

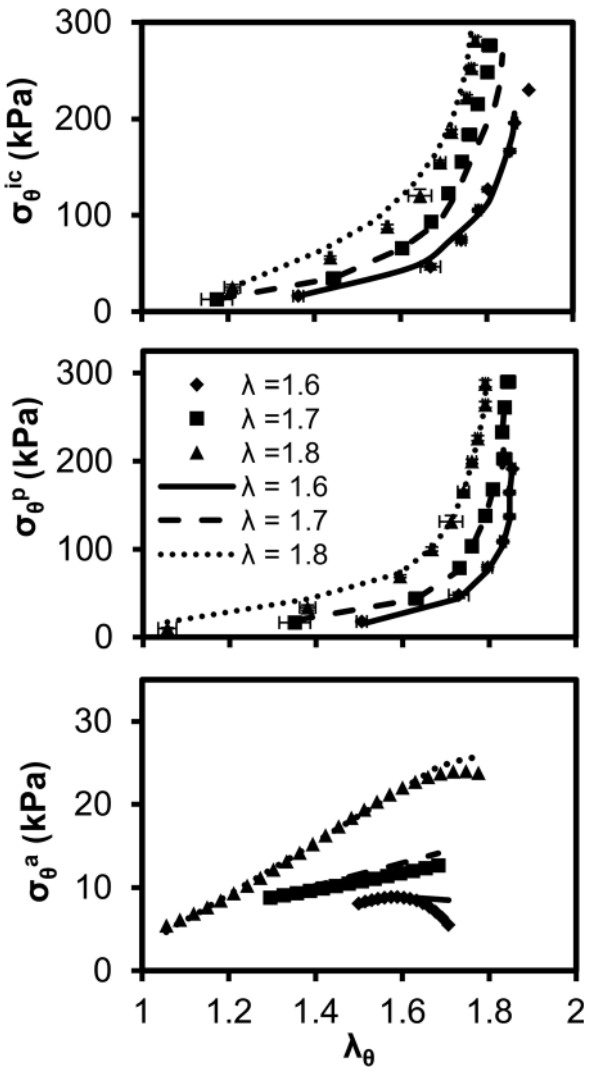

Fig. 2 Representative (top) total stress after isometric contraction (middle), passive stress and (bottom) active circumferential stress–stretch relationships for a porcine common carotid artery at three levels of axial stretch (sample 3). Error bars represent the standard deviation of three repeat measurements on the same vessel. Data points indicate experimentally recorded values, while solid/dashed lines indicate theoretical predictions.

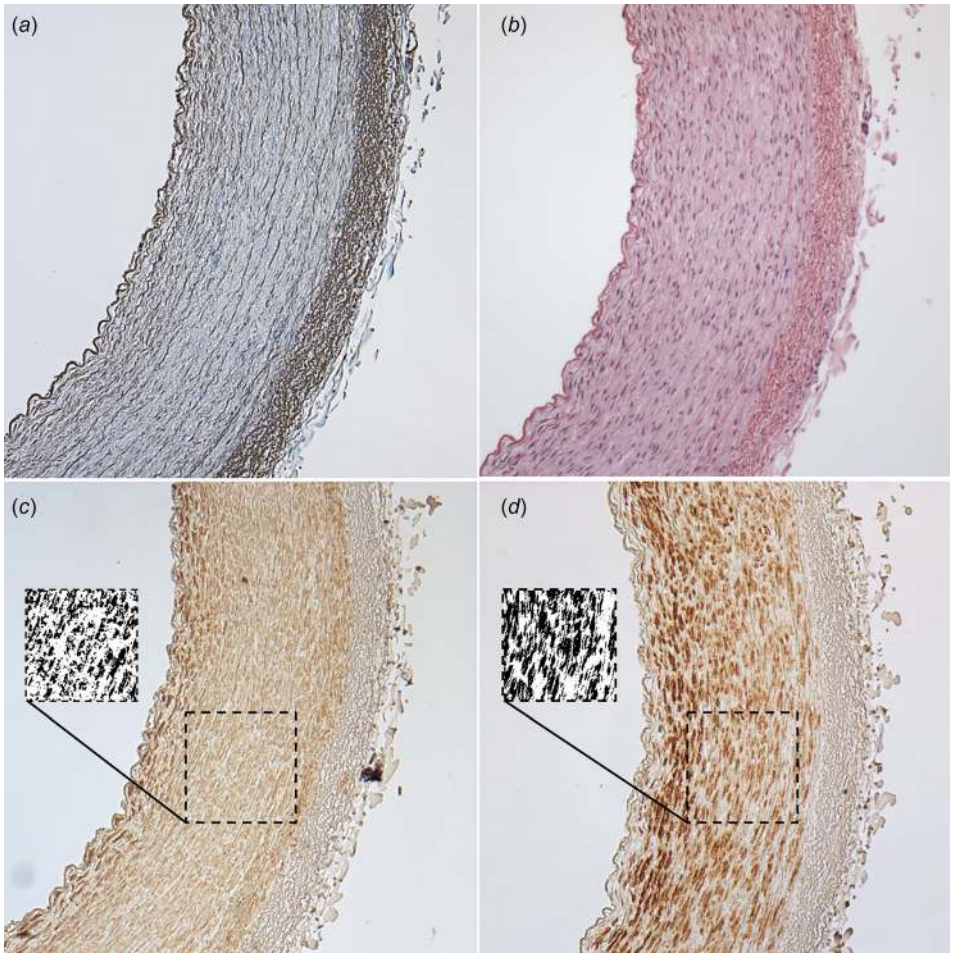

Fig. 3 Histological images (sample 2) of the porcine CCAs at 100× magnification: (*a*) Verhoeff's elastic fiber counterstained with methyl blue, (*b*) Hematoxylin and Eosin, (*c*) smoothelin DAB immunostaining with thresholded inset, and (*d*) smooth muscle-myosin heavy chain DAB immunostaining with thresholded inset

3(*c*) and 3(*d*)) and reported as pixel/pixel density. Moreover, our findings yielded a homogeneous distribution of these subcellular constituents within the media. By staining and analyzing unloaded sections of tissue, it was also assumed that the presence of the contractile markers were independent of mechanical stretch. This may not be the case and future studies would benefit from an analysis of tissues fixed in a deformed state. Still, the overall histological observations are within an acceptable range of other investigators using different analytical techniques [25].

Polynomial regression was performed between active circumferential stress and smoothelin or SM-MHC density (Fig. 4), resulting in an excellent fit for both indicators of contractile phenotype. This relationship helps explain the overall sample-to-sample variation in active stress generation commonly observed in these experiments. We acknowledge sample size limitations in the current study allow for the analysis to contain only six data points. Despite this, both assayed markers of contractile phenotype suggest the capacity to generate active stress reaches a peak around 0.5 (pixel/pixel). Although not reported here, the behavior was also similar when vessels were analyzed at a common pressure (100 mmHg) and axial stretch. We offer the following explanations for this behavior: (i) the physiological stretch conditions used for this correlation may not be at the maxima, (ii) smoothelin and SM-MHC are markers of SMC phenotype but not of the actual contraction itself, (iii) the orientation of SMCs present are not aligned purely in the circumferential direction, or (iv) the matrix stiffens as it contracts. The latter is consistent with nonlinear theory of finite elasticity and represents a common behavior of soft biological materials. Other potential reasons for this curve include biological variability of the specimens and the potential for SMCs damage during the mechanical testing

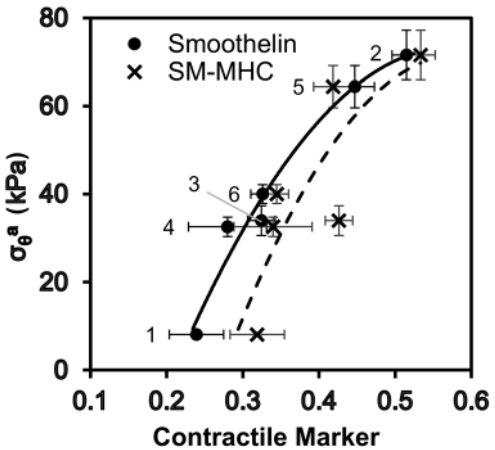

Fig. 4 Second-order polynomial fit between the mean active circumferential stress ($\lambda_\theta = 1.42$, $\lambda_z = 1.6$) and smoothelin (•) and smooth muscle myosin heavy chain SM-MHC (×) density (area positively stained/area all tissue) content in the porcine CCAs. Error bars ± STD mean.

procedure. These factors may be crucial to interpreting the active stress generation in vascular tissues but are outside of the scope of the current analysis.

Common carotid arteries generate active stresses at a lower intensity than the passive stresses under physiological stretches which is in contrast to, but a logical extension of the author's earlier work in muscular renal arteries [4]. Naturally, the carotid artery studied here is of the elastic-type and therefore contains a greater proportion of extra-cellular-matrix proteins [26]. Biochemical modifications to vascular tone play important roles in vascular health and disease [11]. Although our study is not the first to use these (epinephrine and SNP) or other biochemical stimulants to initiate maximally contracted and dilated states, implementation of the biaxial, isometric contraction analysis with the semihybrid two-dimensional/three-dimensional approach and the aforementioned constitutive models represent more recent advances in vascular mechanics [4,5]. This analysis was combined with immmunohistochemistry to provide a novel correlation of SMC contractile phenotype with the capacity to generate contractile stresses.

Conclusion

Using a comprehensive isometric decomposition approach, the passive and active contributions to the total stress state of porcine CCAs have been delineated and correlated with contractile SMC phenotype markers smoothelin and SM-MHC.

Funding Data

- NIH P20GM103499 (JFE, TS), R21EB022131 (JFE), and R01HL222090 (FGS).
- Merit Award from the Veterans' Affairs Health Administration 2I01-BX000168 (FGS).

References

[1] Cox, R. H., 1978, "Regional Variation of Series Elasticity in Canine Arterial Smooth Muscles," Am. J. Physiol., **234**(5), pp. H542–H551.

[2] Dobrin, P. B., 1973, "Influence of Initial Length on Length Tension Relationship of Vascular Smooth Muscle," Am. J. Physiol., **225**(3), pp. 664–670.

[3] Doran, A. C., Meller, N., and McNamara, C. A., 2008, "Role of Smooth Muscle Cells in the Initiation and Early Progression of Atherosclerosis," Arterioscler. Thromb. Vasc. Biol., **28**(5), pp. 812–819.

[4] Zhou, B., Rachev, A., and Shazly, T., 2015, "The Biaxial Active Mechanical Properties of the Porcine Primary Renal Artery," J. Mech. Behav. Biomed. Mater., **48**, pp. 28–37.

[5] Agianniotis, A., Rachev, A., and Stergiopulos, N., 2012, "Active Axial Stress in Mouse Aorta," J. Biomech., **45**(11), pp. 1924–1927.

[6] Cox, R. H., 1975, "Arterial Wall Mechanics and Composition and the Effects of Smooth Muscle Activation," Am. J. Physiol., **229**(3), pp. 807–812.

[7] Dobrin, P. B., 1973, "Isometric and Isobaric Contraction of Carotid Arterial Smooth Muscle," Am. J. Physiol., **225**(3), pp. 659–663.

[8] Fridez, P., Makino, A., Kakoi, D., Miyazaki, H., Meister, J. J., Hayashi, K., and Stergiopulos, N., 2002, "Adaptation of Conduit Artery Vascular Smooth Muscle Tone to Induced Hypertension," Ann. Biomed. Eng., **30**(7), pp. 905–916.

[9] Rachev, A., and Hayashi, K., 1999, "Theoretical Study of the Effects of Vascular Smooth Muscle Contraction on Strain and Stress Distributions in Arteries," Ann. Biomed. Eng., **27**(4), pp. 459–468.

[10] Fonck, E., Prod'hom, G., Roy, S., Augsburger, L., Rufenacht, D. A., and Stergiopulos, N., 2007, "Effect of Elastin Degradation on Carotid Wall Mechanics as Assessed by a Constituent-Based Biomechanical Model," Am. J. Physiol.: Heart Circ. Physiol., **292**(6), pp. H2754–H2763.

[11] Wakatsuki, T., Kolodney, M. S., Zahalak, G. I., and Elson, E. L., 2000, "Cell Mechanics Studied by a Reconstituted Model Tissue," Biophys. J., **79**(5), pp. 2353–2368.

[12] Prim, D. A., Zhou, B., Hartstone-Rose, A., Uline, M. J., Shazly, T., and Eberth, J. F., 2016, "A Mechanical Argument for the Differential Performance of Coronary Artery Grafts," J. Mech. Behav. Biomed. Mater., **54**, pp. 93–105.

[13] Baek, S., Gleason, R. L., Rajagopal, K. R., and Humphrey, J. D., 2007, "Theory of Small on Large: Potential Utility in Computations of Fluid–Solid Interactions in Arteries," Comput. Methods Appl. Mech. Eng., **196**(31–32), pp. 3070–3078.

[14] Zeinali-Davarani, S., Choi, J., and Baek, S., 2009, "On Parameter Estimation for Biaxial Mechanical Behavior of Arteries," J. Biomech., **42**(4), pp. 524–530.

[15] Zhou, B., Wolf, L., Rachev, A., and Shazly, T., 2014, "A Structure-Motivated Model of the Passive Mechanical Response of the Primary Porcine Renal Artery," J. Mech. Med. Biol., **14**(3), p. 1450033.

[16] Taylor, C. R., and Levenson, R. M., 2006, "Quantification of Immunohistochemistry—Issues Concerning Methods, Utility and Semiquantitative Assessment II," Histopathol., **49**(4), pp. 411–424.

[17] Landini, G., 2008, "Advanced Shape Analysis With ImageJ," ImageJ User and Developer Conference, Luxembourg, UK, Nov. 6–7, pp. 116–121.

[18] Nedorost, L., Uemura, H., Furck, A., Saeed, I., Slavik, Z., Kobr, J., and Tonar, Z., 2013, "Vascular Histopathologic Reaction to Pulmonary Artery Banding in an In Vivo Growing Porcine Model," Pediatr. Cardiol., **34**(7), pp. 1652–1660.

[19] Fredersdorf, S., Thumann, C., Ulucan, C., Griese, D. P., Luchner, A., Riegger, G. A. J., Kromer, E. P., and Weil, J., 2004, "Myocardial Hypertrophy and Enhanced Left Ventricular Contractility in Zucker Diabetic Fatty Rats," Cardiovasc. Pathol., **13**(1), pp. 11–19.

[20] Eberlov, L., Tonar, Z., Witter, K., Kkov, V., Nedorost, L., Koraben, M., Tolinger, P., Koov, J., Boudov, L., Teka, V., Houdek, K., Molek, J., Vrzalov, J., Peta, M., Topolan, O., and Valenta, J., 2013, "Asymptomatic Abdominal Aortic Aneurysms Show Histological Signs of Progression: A Quantitative Histochemical Analysis," Pathobiology, **80**(1), pp. 11–23.

[21] van der Loop, F. T. L., Gabbiani, G., Kohnen, G., Ramaekers, F. C. S., and van Eys, G. J. J. M., 1997, "Differentiation of Smooth Muscle Cells in Human Blood Vessels as Defined by Smoothelin, a Novel Marker for the Contractile Phenotype," Arterioscler. Thromb. Vasc. Biol., **17**(4), pp. 665–671.

[22] Rensen, S. S. M., Doevendans, P. a F. M., and van Eys, G. J. J. M., 2007, "Regulation and Characteristics of Vascular Smooth Muscle Cell Phenotypic Diversity," Neth. Heart J., **15**(3), pp. 100–108.

[23] Hao, H., Gabbiani, G., and Bochaton-Piallat, M.-L., 2003, "Arterial Smooth Muscle Cell Heterogeneity: Implications for Atherosclerosis and Restenosis Development," Arterioscler. Thromb. Vasc. Biol., **23**(9), pp. 1510–1520.

[24] van Eys, G. J., Niessen, P. M., and Rensen, S. S., 2007, "Smoothelin in Vascular Smooth Muscle Cells," Trends Cardiovasc. Med., **17**(1), pp. 26–30.

[25] Roy, S., Silacci, P., and Stergiopulos, N., 2005, "Biomechanical Proprieties of Decellularized Porcine Common Carotid Arteries," Am. J. Physiol.: Heart Circ. Physiol., **289**(4), pp. H1567–H1576.

[26] Berne, R. M., and Levy, M. N., 2001, *Cardiovascular Physiology*, Mosby, St. Louis, MO.